Simple, *Simple Post-Stall Aerodynamic Model*

An **abridged** version of the report "*Simple Post-Stall Aerodynamic Model*" produced in the 2019-2020 academic year by D. Clifford at the University of Southampton

V1.0

16/08/2020

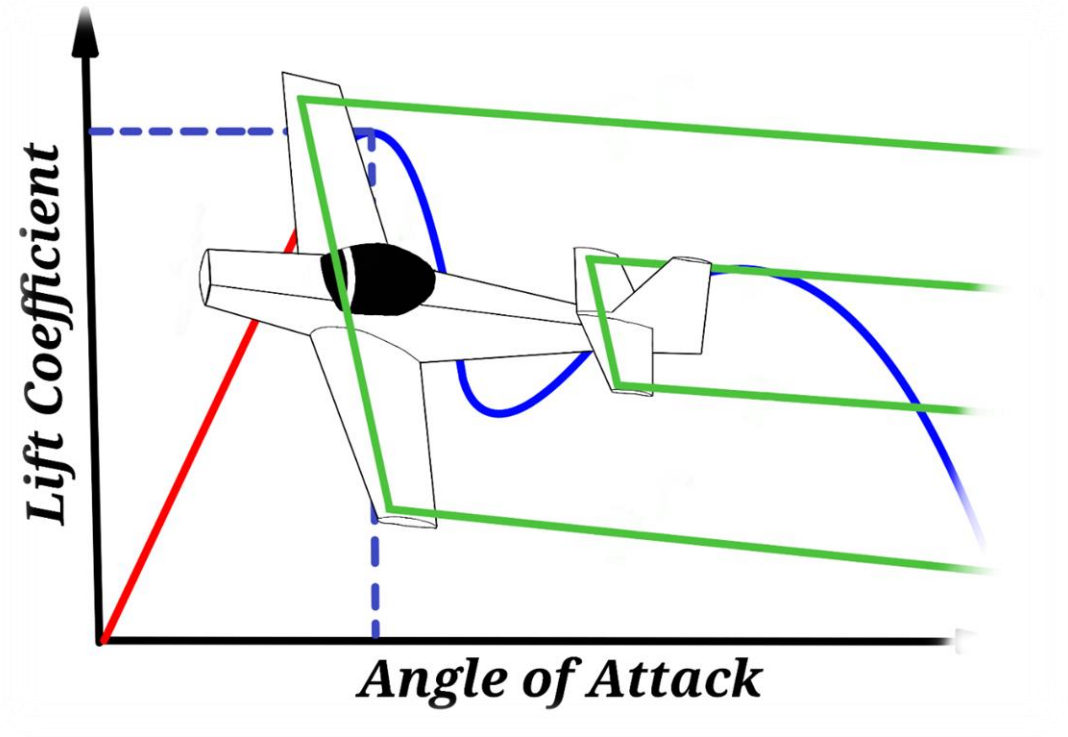

For this project's code and more of my work see my GitHub profile:

https://github.com/DeclanClifford

Abstract

The project saw the creation of a numerical nonlinear aerodynamic method with a simplified flow model. The method, which models a lifting surface using a single horseshoe vortex to account for 3D flow was coupled with 2D sectional lift coefficient data which includes stall and post-stall regions. The resultant model gives lift and induced drag results over a 360-degree range. The single horseshoe vortex model was able to produce converged results for aspect ratios greater than two, and furthermore, had exact agreement with the analytical result of Prandtl's Lifting Line Theory for a moderate to large aspect ratio wing with an elliptical lift distribution. The model produces the expected behaviour at stall and post-stall though slightly overestimates maximum lift coefficient due to the simplicity of the model.

1 Contents

2 Author's Note

This is a **modified and abridged** version of a report I produced in my third year of study at the University of Southampton. The original report focused on the creation of a simple nonlinear aerodynamic model with post-stall capability, which could be used as a teaching aide for second year aerospace students and could be coupled with a longitudinal flight simulator. It was my intention while writing this new report to produce something less formal and less intimidating than the original 78-page report, ideally something around 10 pages long. **This short(er) report focuses on the theory of the first half of the original text, and furthermore limits discussion to the simplest form of model, the single horseshoe vortex model. Much of the testing and validation of the model can be found in the original report and so only the most basic cases are given here**. Soon I will create another short(ish) report highlighting the flight simulator portion of my original report.

3 Background

Much of classical aerodynamic theory works on the assumption of linear relationships. Among the most well-known is Prandtl's Lifting Line theory, developed by Ludwig Prandtl in the early 20th century to predict the aerodynamic properties of finite wings [1]. The lifting line method has proved itself an extremely robust method for predicting pre-stall aerodynamic properties and is still used by engineers in the present day as a preliminary design tool [1]. Engineers of the present have become more interested in nonlinear aerodynamics, that is the stall and post-stall behaviour of a lifting surface. Developing an understanding of these nonlinear behaviours has an important part of much aircraft design, especially during the preliminary design phase. Safety is always at the forefront of aircraft design, and predicting this stalled behaviour, and knowing how the aircraft will react, is critical to making a safe design and a design that does not come with later unforeseen handling characteristics. Understanding this stalled behaviour

however presents a different challenge. Von Karman is stated to have proved that post-stall, the solutions of lifting line theory become nonunique such that there are an infinite number of solutions [2]. Most other classical aerodynamic models face this same problem and are not suitable for use in predicting stalled behaviour without undergoing some form of modification. Much work has already been done in this field with many such modifications being made, leading to nonlinear methods of varying complexity.

This short report focuses on an adaption of Anderson's numerical nonlinear lifting-line method [3]. The reason for choosing to work with this method above other well established and more complex methods lies partly within the scope of the original report, "*Simplified Post-Stall Aerodynamic Model*" which was to create a simple aerodynamic model which had the potential to be used as a teaching aide for second year aerospace university students.

4 Review of Key Concepts

Before continuing it is necessary to cover the key concepts used to create the model.

4.1 The Finite Wing – Spanwise flow and local velocity

An important distinction to make is the difference between a wing and an aerofoil. Wings are 3D bodies of finite span. Aerofoils on the other hand are 2D bodies. This means that aerofoils do not experience the component of fluid flow in the spanwise direction that finite wings do. The absence of this spanwise component prevents the modelling of the flow "spilling" over the wing tips, from the lower high-pressure surface to the upper low-pressure surface. The result of the spanwise flow is a trailing vortex, generated along the wing tips.

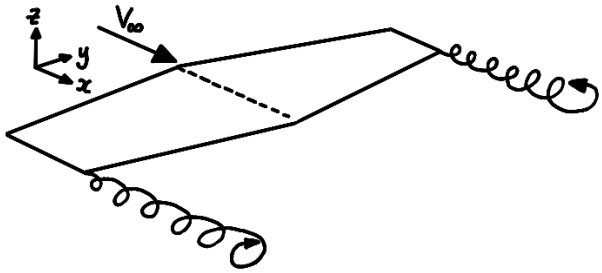

Figure 1: Wingtip vortices schematic

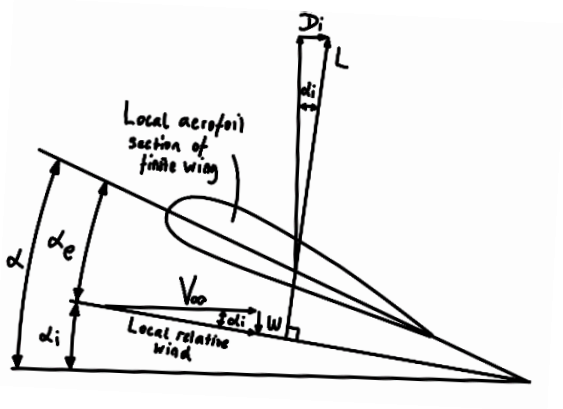

Figure 2: Downwash effect over a finite wing section

These trailing vortices generate a downward velocity component known as downwash. This interacts with the free stream velocity, creating a local velocity which acts at an angle downwards of the free stream velocity. This angle is known as the induced angle of attack, and has the equation

$$\alpha_i = \tan^{-1}\frac{w}{V_\infty} \tag{1}$$

where w is the induced velocity of the trailing vortices, known as downwash, and V_∞ is the free stream velocity. The angle of attack of the aircraft is now redefined as the geometric angle of attack, α, since the angle of attack the local stream velocity experiences over the wing is adjusted by the induced angle of attack. This angle is known as the effective angle of attack, and can be found as

$$\alpha_e = \alpha - \alpha_i \tag{2}$$

An important part of this theory is stated by Gallay & Laurendeau [4], who say that the sectional lift coefficient at an effective angle of attack is the same as the lift coefficient of the finite wing at its corresponding geometric angle of attack. This is part of the theory that allows 2D sectional data to be coupled with a method to model a finite wing.

4.2 Vortex Filaments

With this information, a highly simplified model of a lifting surface can be created by modelling it as a horseshoe vortex. The horseshoe vortex is composed of vortex filaments which are lines in 3D space about which there are circulations. The Helmholtz theorems [5] state that firstly vortex filaments do not end in a fluid, and that secondly, vortex filaments have constant circulation along their length. Arranging vortex filaments into a horseshoe shape allows a lifting surface to be modelled in 3D space. Two vortex filaments extend to infinity, approximating the trailing vortices and bounding another vortex filament between them. The bound vortex follows the lifting surface's aerodynamic centre, which can be assumed to be at the quarter chord point of most aerofoils.

Using the Biot Savart Law [5], velocity induced by a vortex filament at a point can be determined as

$$w = \frac{\Gamma}{4\pi} \frac{\boldsymbol{r}_{AC} \times \boldsymbol{r}_{BC}}{|\boldsymbol{r}_{AC} \times \boldsymbol{r}_{BC}|^2} \boldsymbol{r}_{AB} \cdot \left(\frac{\boldsymbol{r}_{AC}}{r_{AC}} - \frac{\boldsymbol{r}_{BC}}{r_{AC}} \right) \tag{3}$$

where bold typeface denotes a vector and otherwise, a scalar.

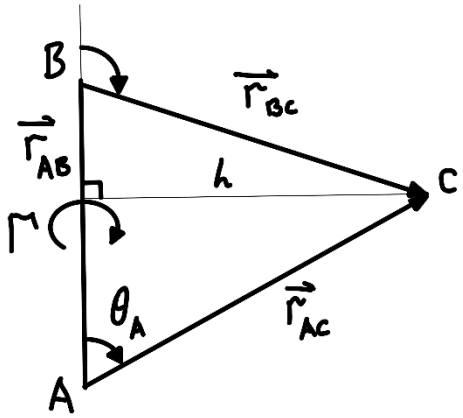

Figure 3: Geometry to illustrate the velocity at point C due to a segment AB of a vortex filament

4.3 The Kutta-Joukowski Theorem

Another important theorem used is the Kutta-Joukowski Theorem [6]. This is another part of the theory that allows 2D sectional aerofoil data to be coupled with the 3D numerical method.

The theorem states that for a 2D body, lift per unit span is directly proportional to circulation around the body

$$L' = \rho_\infty V_\infty \Gamma \tag{4}$$

where ρ_∞ is the density of the free stream flow. Taking the equation for sectional lift coefficient

$$C_l = \frac{L'}{0.5\rho_\infty {V_\infty}^2 c} \tag{5}$$

where c is the wing chord and rearranging for the lift per unit span, an equation for circulation can be found in terms of the sectional lift coefficient, free stream velocity and wing chord.

$$\Gamma = \frac{C_l V_\infty c}{2} \tag{6}$$

5 Finite Wing Numerical Method

5.1 Defining the Model's Geometry – the Single Horseshoe Vortex Model

Using the theory outlined in the previous section, a simple model of a lifting surface can be created.

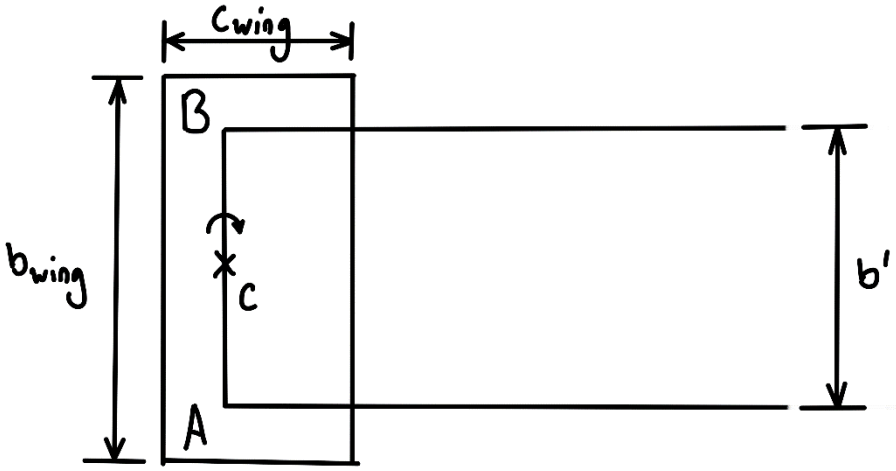

Figure 4: Geometrical representation of the single horseshoe vortex system modelled in this project

The model, shown in Figure 4 consists of three vortex filaments. The vortex filaments from $A{-}A_\infty$ and $B - B_\infty$ act as the wing's trailing vortices. These are bounded by a central horseshoe vortex $A - B$ which runs along the span of the wing.

It is important to discuss the location of the control point, C. In other aerodynamic methods such as the vortex lattice method, the inductions of all three vortex filaments are considered at the control point and a system of equations can be solved, after having imposed boundary conditions, to find the circulation. This means the model would have two free parameters; the distance between the trailing vortices, b' and the chordwise location of the control point, c'. The method used in this project follows classical lifting line theory, using the downwash from the trailing vortices to find the induced angle of attack, and using this to find the effective angle of attack. This means the method used here has only one free parameter, b'. The value of this parameter can be used to satisfy certain conditions. One useful theorem to match is the slender wing result [5], which states that the lift curve slope of a low aspect ratio wing follows

$$a_w = \frac{\pi AR}{2} \tag{7}$$

where AR is the wing's aspect ratio. To match this result, b' must be set to equal

$$b' = \frac{b}{\sqrt{2}} \tag{8}$$

where b is wingspan. Proving this is mostly an exercise of algebra and so is not included in this report. A detailed proof of this result can be found in [5], which covers a more complex vortex lattice method model.

5.2 Methodology

The methodology behind the numerical model of this report can be described as follows:

1. An initial angle of attack, α_{geo} is assumed and the sectional lift coefficient, C_l corresponding to this angle is called from a known sectional lift coefficient plot. The subscript $_{geo}$ is only used to clarify that this is the geometric angle of attack and does not change throughout the iterative process. A circulation, Γ is then calculated using Eq. (6). Care should be taken here since Eq. (4) considers lift per unit span, L', as $\frac{L}{b}$. When adapting this to the horseshoe vortex model, lift per unit span should be taken as $\frac{L}{b'}$. This means Eq. (6) will be multiplied by a factor of $\sqrt{2}$ for this model.

2. Γ is then used to determine the induced velocity at the control point C, shown in Figure 4. As stated in the previous section, only the downwash from the trailing vortices is considered. Combining these inductions lets the induced velocity from the two trailing vortices be expressed as

$$w_i = \frac{-\Gamma}{\pi b'} \tag{9}$$

3. The induced angle of attack can then be determined using the relation

$$\alpha_i^0 = \tan^{-1}\frac{w_i}{V_\infty} \tag{10}$$

where the superscript ^{0} denotes an initial guess.

4. With the induced angle of attack, a first guess for the effective angle of attack can be made as

$$\alpha_e^0 = \alpha_{geo} - \alpha_i^0 \tag{11}$$

where α_{geo}, the input angle, is the angle an effective angle of attack is desired to be determined at. α_i^0 is the induced angle of attack found in step 3. If the value of α_e^0 is zero, steps 5 and 6 concerning the iterative angle of attack correction process can be skipped and α_e^0 can be considered as the converged effective angle of attack used in step 7.

5. A new induced angle of attack, α_i^{n+1} is now calculated using the same method as outlined in steps 1 – 3, though this time the C_l in step 1 is found at the newest effective angle of attack, α_e. For the initial calculation this will be α_e^0. For subsequent iterations this will be α_e^{n+1} found in step 6.

6. A new effective angle of attack can now be found as

$$\alpha_e^{n+1} = \phi\alpha_e^n + \phi\left(\alpha_{geo} - \alpha_i^{n+1}\right) \tag{12}$$

where ϕ is a relaxation factor used to help the rate of convergence. Here $\phi = 0.5$. This method calculates a new effective angle of attack and makes use of the result of the previous iteration to increase the rate of convergence. Steps 5 and 6 should be repeated until the condition $\left|\frac{\alpha_e^n - \alpha_e^{n+1}}{\alpha_e^n}\right| \leq tol$ is met, where tol is a user specified tolerance and in this report is set to 0.25%, then this final result can be considered as the converged effective angle of attack, α_e^{con}, and no further iterations are required.

7. Using the same process as in step 1, a new sectional lift coefficient, C_l^{con} is determined, though this time at α_e^{con}. Then, using Eq. (6) the circulation at the geometric angle of attack, α_{geo}, corrected for the effects of downwash can be found as

$$\Gamma^{con} = \frac{C_l^{con} V_\infty c}{2} \tag{13}$$

Inserting Γ^{con} into the equation in step 2 yields the converged downwash velocity vector, $\boldsymbol{w}_i^{con}$. The local velocity vector can then be found as

$$\boldsymbol{u} = \boldsymbol{V} + \boldsymbol{w}_i^{con} \tag{14}$$

where $\boldsymbol{V}$ is the free stream velocity vector and can be expressed in column vector form as

$$\boldsymbol{V} = \begin{bmatrix} V_\infty \cos\alpha_{geo} \\ 0 \\ V_\infty \sin\alpha_{geo} \end{bmatrix} \tag{15}$$

It is important to note the velocity vector is taken **relative to the lifting surface's datum line** (wing chord line) in this model.

For the sake of clarity, the downwash velocity vector $\boldsymbol{w}_i^{con}$ can be expressed in column vector form as

$$\boldsymbol{w}_i^{con} = \begin{bmatrix} 0 \\ 0 \\ \dfrac{-\Gamma^{con}}{\pi b'} \end{bmatrix} \tag{16}$$

With the local velocity found, the resultant force and its direction can be determined using a cross product of the local velocity and bound vortex segment direction, which in this case is taken as $\boldsymbol{r}_{AB}$

$$\boldsymbol{F} = \Gamma^{con}\rho(\boldsymbol{u} \times \boldsymbol{r}_{AB}) \tag{17}$$

where ρ is the fluid's density. This equation can be split into its respective x and z axis components F_x and F_z, which are the body forces of the lifting surface. Lift and induced drag can be found by resolving these forces with respect to the lifting surface's angle of attack as

$$L = F_z \cos \alpha_{geo} - F_x \sin \alpha_{geo} \tag{18}$$

$$D_{ind} = F_x \cos \alpha_{geo} + F_z \sin \alpha_{geo} \tag{19}$$

6 "Sectional Lift Coefficient Data"

A common theme in this report is sectional aerofoil data. Without sectional aerofoil data which includes the stall and post-stall regions, the methodology described above is quite useless. This type of aerofoil data can be difficult to find in great variety. This report saw to the creation of sectional lift coefficient data that spanned 360 degrees of rotation by blending thin aerofoil theory and flat plate theory [7] with a hyperbolic blending function. This method allowed for the fast creation of approximate sectional lift coefficient plots that spanned the full range of rotation requiring at the very most pre-stall XFOIL results. The finer details of this aerofoil data generation method go beyond the intended purpose of this simplified report and so will not be discussed here.

7 Results

Before looking at the results, some limitations of the model must be discussed. This method is restricted to modelling straight rectangular wings of moderate to large aspect ratios. This is due to the model using only one horseshoe vortex and the limitation of classical lifting line theory (which this methodology is based off) to only produce acceptable results for wing aspect ratios greater than 4. Furthermore, this model only considers the net forces of the lifting surface and is unable to model lift distributions. The full version of this report goes into greater detail, expanding this methodology to an N-element model. The N-element model sees success

demonstrating spanwise circulation distributions pre- and post-stall with larger numbers of horseshoe vortices and can accurately model the effects of wing taper.

7.1 Theoretical Comparison

A simple way to test the model is to see how it compares with one of the more popular results of lifting line theory, that is the lift slope of a high aspect ratio straight wing with an elliptical lift distribution [5]. This result is given by

$$a_w = \frac{2\pi}{1 + \frac{2\pi}{\pi AR}} \tag{20}$$

where a_w is the lift curve slope and AR is the aspect ratio.

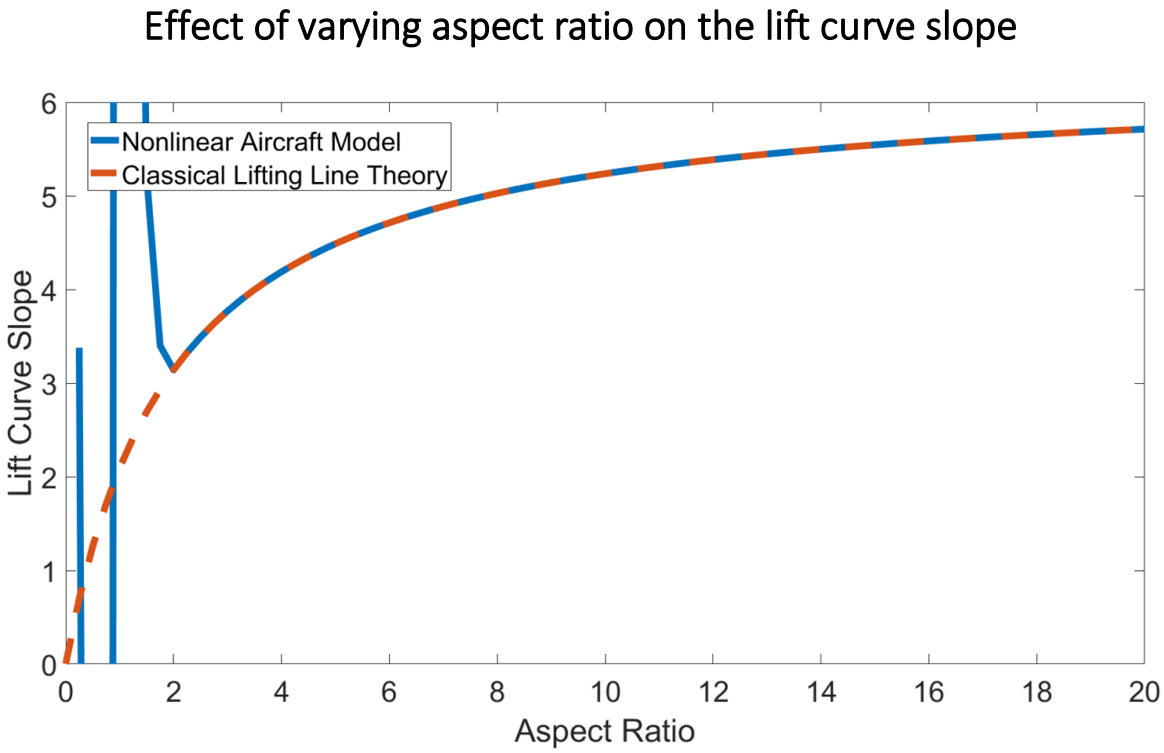

Figure 5: A comparison between the nonlinear single horseshoe vortex model and the analytical result of classical lifting line theory

Looking at Figure 5, the nonlinear single horseshoe vortex model matches the analytical result given above exactly for aspect ratios greater than 2. This is good proof of the functionality of the model. The noticeable divergence of the lift curve slope at small aspect ratios is due to the very simple sectional data coupling method employed. More complex coupling, and iterative, methods have been proposed [4], though at the cost of significantly increasing the model's complexity. These small aspect ratios are however beyond the range of what lifting line theory would be used to predict, and beyond the range of what most conventional aircraft may use.

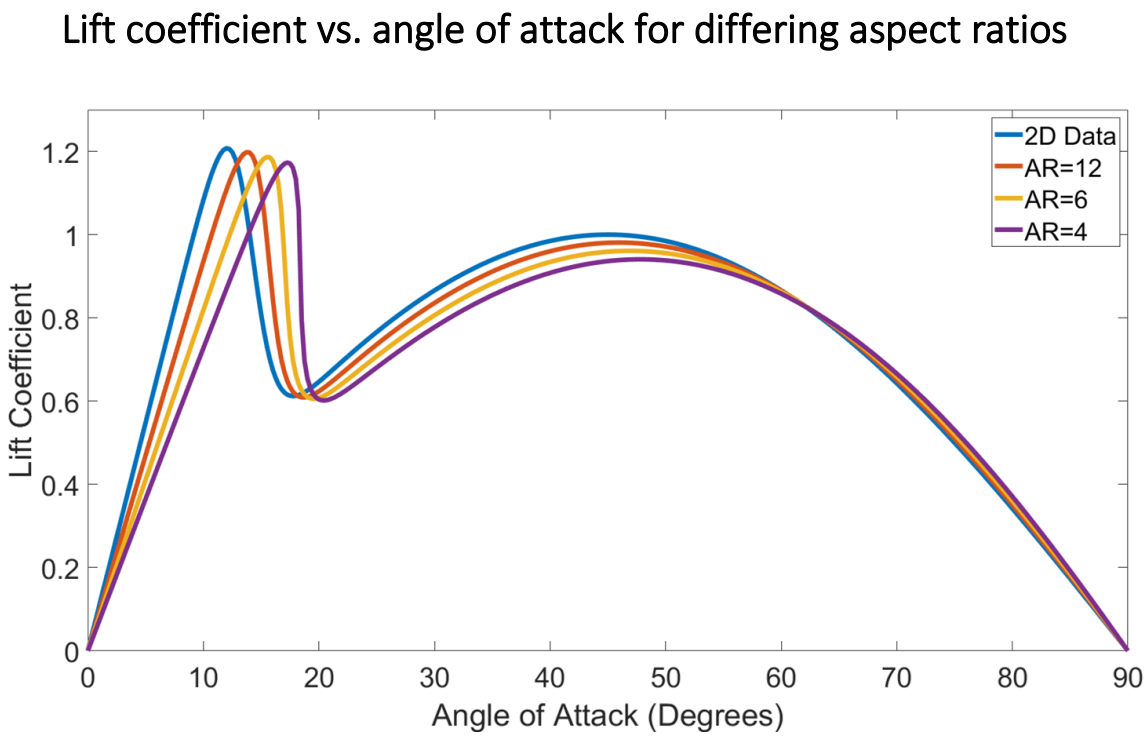

Figure 6: Single horseshoe vortex nonlinear model - Lift coefficient vs angle of attack rectangular planform wings of different aspect ratio.

Another useful result to see is lift coefficient variation with angle of attack. Figure 6 shows this for several aspect ratios and shows the original sectional data input. The model produces the expected behaviour where the stall point is delayed with increasing aspect ratio. The expected decrease in maximum lift coefficient can also be seen. At very high angles of attack, the results of the nonlinear model tend towards the original sectional input. This is because downwash effects decrease as the wing approaches 90 degrees and the local velocity matches the free stream velocity. It's important to note now that in this model the trailing vortices have been aligned with the free stream velocity. This is done since the model functions at very high angles of attack and so the assumption of only small angle use is not valid. The effect of this alignment is not significant in this form of the model since it uses only one horseshoe vortex, and models only one lifting surface. The original report goes into more detail on this subject and looks at wing and tail configurations for a flight simulator.

8 References

[1] J. Anderson, Fundamentals of Aerodynamics, 6th Edition, New York: McGraw-Hill Education, 2017, p. 436

[2] D. Hunsaker, "A Numerical Vortex Approach to Aerodynamic Modelling of SUAV/VTOL Aircraft", M.S. Thesis, Brigham Young University, Utah, USA, April 2007, p.34, [Online]. BYU Scholars Archive, https://scholarsarchive.byu.edu/cgi/viewcontent.cgi?article=2070&context=etd [Accessed: 03 Feb 2020]

[3] J. Anderson, Fundamentals of Aerodynamics, 6th Edition, New York: McGraw-Hill Education, 2017, pp.465-468

[4] S. Gallay and E. Laurendeau, "Nonlinear Generalized Lifting-Line Coupling Algorithms for Pre/Poststall Flows", AIAA Journal, Vol. 53, No. 7, July 2015, p. 1785, [Online]. Available: ARC AIAA, https://doi.org/10.2514/1.J053530 [Accessed: 16 Mar 2020]

[5] N. Sandham, Class Lecture, "Vortex Lattice Methods", SESA3033, Faculty of Engineering & Environment, University of Southampton, Southampton, UK, 2005-2006, pp. 25-27

[6] J. Anderson, Fundamentals of Aerodynamics, 6th Edition, New York: McGraw-Hill Education, 2017, p. 440

[7] J. Tangler and J. Kocurek, "Wind Turbine Post-Stall Airfoil Performance Characteristics Guidelines for Blade-Element Momentum Methods," in *43rd AIAA Aerospace Sciences Meeting and Exhibit*, Reno, Nevada, USA, January 10-13, 2005 [Online]. Available: AIAA ARC, https://doi.org/10.2514/6.2005-591 [Accessed: 05 Feb 2020]